Development of a Hydraulic Manipulator Servoactuator Model: Simulation and Experimental Validation

Glen Bilodeau
gbilod@cim.mcgill.ca

Evangelos Papadopoulos
egpapado@cim.mcgill.ca

Department of Mechanical Engineering & Centre for Intelligent Machines
McGill University,
Montreal, QC, Canada H3A 2A7

Abstract

In this paper, modelling and identification of a hydraulic servoactuator system is presented. The importance of such a model is evident in further understanding the system and in order to develop a robust force controller. The model accounts for line losses, nonlinear orifice areas, hysteresis, friction, leakage, and load dynamics. System parameters are identified based on a high-performance hydraulic manipulator joint, and in particular, the elbow of the SARCOS slave manipulator. Specialized hardware was designed and constructed in order to help identify parameters, to allow line pressure measurements, and to validate the model. The model is verified by comparing simulation and experimental results in two modes: static and dynamic. The results prove to be very good. The developed model sheds light onto the subsystems in a hydraulic manipulator joint and will prove useful in the development of a robust force control algorithm.

1 Introduction

Interaction with an environment, workpiece, or tool is the basis of many tasks performed by humans. As a result, there is motion through free space and applied forces in the case of contact. Some tasks pose a danger to humans, for example, hazardous waste management, space and planetary exploration, and live-line maintenance of electrical wires. Automation or teleoperation of such tasks would distance humans from dangerous sites and allow a safe and efficient task completion.

Applying forces with automated or teleoperated manipulators is a very complex task. The task may require the robot to apply large forces on an environment which may be rigid or flexible, and stationary or oscillating. If the manipulator is located on a vehicle or on a long boom, its base will not be completely immobilised but will be subject to flexibility-induced disturbances or vibrations. Furthermore, the robot itself will also demonstrate some degree of flexibility due to actuator, sensor, and possibly link dynamics. Of special interest are manipulators with electrohydraulic actuation. Such manipulators are advantageous for the tasks described above because of their high torque to weight ratio, their inertance to fire hazards, and the availability of hydraulic power in mobile applications.

Much research in automated or teleoperated control of manipulators deals with electrically actuated manipulators. In contrast, less work has been done on electrohydraulically actuated manipulators. Previous research span both modelling and control of hydraulic actuators. With respect to modelling, some works deal with the traditional spool type valve, for which in most cases, the orifice areas are linear with respect to the valve position. In contrast, the jet-pipe/suspension type servovalves are more complex. One advantage of this type of servovalve is that there is no contact between surfaces as there is between the spool and spool housing in the spool valve. Another advantage is that the valve moving parts are small, and therefore high bandwidths can be achieved. For the jet-pipe servovalve, a detailed model is proposed in [3] and [11].

In terms of control of hydraulic actuators, modelling the physical effects is important. In previous works, position and force control have been studied. A linearized model was used for position control of a spool-valve and rotary actuator system [7]. A model is used in a feedforward simulation filter (an alternative to the inverse dynamics method) for control of a hydraulically actuated flexible manipulator [9]. Force control is more difficult in the case of hydraulic actuators since the current input modulates valve resistance rather than a torque (as in the case of an electrical actuator). Use of a model of a hydraulic system to evaluate the hybrid position/force control scheme, inherently not model-based, is demonstrated by [2], [5], [13] and explicit force control, for example, by [3], [10]. The impedance control law, which is model-based, is applied to a hydraulic manipulator in [6]. Although the focus is on control, modelling is essential in understanding the system to be controlled. One way of obtaining a faithful and robust controller is to include a model-based portion in order to reduce control effort.

This paper deals with the accurate modelling of the elbow joint of a small slave SARCOS dexterous manipulator. The developed model includes hysteresis, orifice areas, damping, and leakage. To date, no model of a hydraulically actuated joint which includes servovalve and rotary actuator dynamics is available in the literature. Although not discussed in this paper, the ultimate purpose of our modelling work is to develop a controller, to gage controller perfor-

mance in simulation and to improve controller performance experimentally.

The paper is organized as follows: in Section 2 the subsystems are discussed including the major physical effects that are found. System equations are given. Section 3 describes the experimental setup and discusses the parameters identified and the procedures used. Section 4 compares experimental results with simulation results, validating the model. Finally, conclusions are given in Section 5. Table I describes the notation used in this paper.

2 Physical Modelling

Subsystems that are modelled in this research work include the servovalve, the hydraulic lines, the rotary actuator, and the load. The dynamics of the valve tip and the hysteresis in the servovalve are considered. The various subsystems are shown in Figure 1. The servovalve is composed of a moving element actuated by a small torque motor. Input current modulates the position of the valve opening supply and return orifices, allowing flow to enter and leave the actuator. In electric direct-drive motors, the torque is directly proportional to the amplifier input allowing the motor to act as a source of torque. The hydraulic line losses are represented by linear resistances assuming laminar flow. Fluid inertance due to fluid mass in the lines, and fluid capacitance are also taken into consideration [1] [12]. The load and its shaft is represented by simple components, that is, by a mass-spring-damper, as needed. The friction in the joint is modelled as Coulomb friction, to account for stick-slip effect.

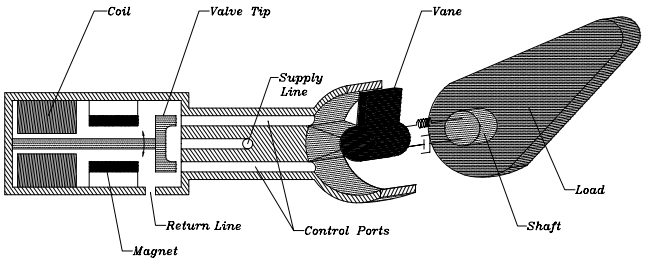

Fig. 1. Joint and valve schematic.

Of importance is the flow through the orifice as the valve tip position is changed. Here, the flow is turbulent and the relation between the flow and effort variables (flow rate and pressure) is a square-root law, i.e. a non-linear resistance. This can be represented as,

$$Q = C_d A_{orifice}(x_v)\sqrt{\frac{2}{\rho}\left(P_{hi} - P_{lo}\right)} = g_{orifice}(x_v, P_{hi}, P_{lo}) \quad (1)$$

Also, since the direction of flow changes as a result of the valve position, flow forces result. These tend to close an opening valve, and in the case of a suspension valve may also lead to a slight offset in the valve position [1]. For the jet-pipe valve, although a flow-force model is proposed [11], a suitable physically-based characterization of the flow forces is not available. Here, the flow forces represent the change in momentum as fluid flows through the orifices creating regions of high pressure and low pressure.

Table I. Nomenclature.

Variable	Definition
i, i_{hys}	current before and after hysteresis.
I_v, B_v, K_v	servovalve suspension arm moment of inertia, damping, and stiffness.
θ_v, x_v	suspension arm angular displacement, valve tip displacement.
l_p	length of suspension arm.
B	servovalve motor torque constant.
ρ, μ, β	density, viscosity and bulk modulus of oil.
A_s, l_s, d_s	cross-sectional area, length and diameter of supply line.
A_r, l_r, d_r	cross-sectional area, length and diameter of return line.
P_s , P_r	pump pressure and tank pressure.
Q_{sv}, P_{sv}	flow through supply line, supply pressure before servovalve.
P_{sv2}	pressure at valve tip.
Q_{rl}, P_{rl}	flow through return line, return pressure after servovalve.
P_{p1} , P_{p2}	chamber pressures, port 1 and port 2.
V_{n1} , V_{c1}	volume in line of port 1 and in chamber 1.
V_{p2} , V_{c2}	volume in line of port 2 and in chamber 1.
C_d	discharge coefficient.
D_v	rotary actuator volumetric displacement.
R_v	leakage coefficient of rotary actuator.
J_v , J_l	vane and load rotary inertia.
b_{vn}, b_l, b_s	vane, load and shaft damping.
k_s	shaft angular stiffness.
ω_{vn}, θ_{vn}	vane angular velocity and angular position.
ω_l, θ_l	load angular velocity and angular position.
τ_{ext}, τ_{coul}	external torque and torque due to friction.
W_l	weight of load
C_A	accumulator capacitance
τ_{ff}	torque due to flow force at valve tip.

Due to the magnetics in the torque motor, the relation between the input current and the valve tip position is hysteretic. In order to mathematically represent this phenomenon, a model based on the Jiles-Atherton theory for magnetization of ferromagnetic material is used [4]. A differential equation yields both major and minor loops, and is suitable for incorporation into the overall system model for simulation. Only the initial point of each part of the curve is required to find the solution. In essence, this adds one differential equation to the system model.

The bond graph approach (systems approach) is used to derive the system dynamic models. The bond graph essentially represents the power bonds between subsystems. It establishes the way subsystems are bonded together, the effort and flow variables at the ports of the subsystems, and sign conventions for power flow. With this approach, each subsystem is composed of basic one-port and two-port elements representing the physical effects within the subsystem. These elements include resistances, inertances (inductances), capacitances, transformers and gyrators. The various multi-port elements interact via three-port junction elements. Finally, compatibility and continuity laws are

applied to obtain the system equations [8]. In all, the bond graph approach allows for a unified and efficient representation of multi-domain systems.

The application of continuity and compatibility laws, along with individual element equations, leads to a set of nonlinear first order differential equations which needs to be solved. The system bond graph is shown in Figure 2 and the equations of motion are given as,

Hysteresis:

$$\dot{i}_{hys} = f_{hys}(i, \dot{i}, i_{hys}, t) \tag{2}$$

Valve Tip:

$$I_v \ddot{\theta}_v + B_v \dot{\theta}_v + K_v \theta_v = B i_{hys} + \tau_{ff} \tag{3}$$

$$x_v = l_p \theta_v \tag{4}$$

Flow Equations: (Line, Servovalve, Actuator)

$$\dot{Q}_{sv} = \frac{A_s}{\rho l_s}\left(P_s - \frac{128 \mu l_s}{\pi d_s^4} Q_{sv} - P_{sv} \right) \tag{5}$$

$$\dot{P}_{sv} = \frac{1}{C_A}\left(Q_{sv} - g_{lk}(x_v, P_{sv}, P_{rl}) - g_v(x_v, P_{sv}, P_{sv2}) \right) \tag{6}$$

$$\dot{P}_{p1} = \frac{\beta}{(V_{c1} + V_{p1})}\left(g_1(x_v, P_{sv2,} P_{p1}) - g_4(x_v, P_{p1}, P_{rl}) - D_v \omega_{vn} - R_v(P_{p1} - P_{p2}) \right) \tag{7}$$

$$\dot{P}_{p2} = \frac{\beta}{(V_{c2} + V_{p2})}\left(g_2(x_v, P_{sv2}, P_{p2}) - g_3(x_v, P_{p2}, P_{rl}) + D_v \omega_{vn} + R_v(P_{p1} - P_{p2}) \right) \tag{8}$$

$$\dot{Q}_{rl} = \frac{A_r}{\rho l_r}\left(P_{rl} - \frac{128 \mu l_r}{\pi d_r^4} Q_{rl} - P_r \right) \tag{9}$$

Vane and Load:

$$\dot{\omega}_{vn} = \frac{1}{J_v}\left(D_v(P_{p1} - P_{p2}) - \tau_{coul}(\omega_{vn}) - b_{vn}\omega_{vn} - k_s(\theta_{vn} - \theta_l) - b_s(\omega_{vn} - \omega_l) \right) \tag{10}$$

$$\dot{\omega}_l = \frac{1}{J_l}\left(k_s(\theta_{vn} - \theta_l) + b_s(\omega_{vn} - \omega_l) - \tau_{coul}(\omega_l) - b_l\omega_l - W_l \sin(\theta_l) + \tau_{ext} \right) \tag{11}$$

The two dependent variables, P_{sv2} and P_{rl}, are cumbersome to solve for assuming the square root law. To ease computation and solution, linear resistances were assumed. They can be found through compatibility equations at their respective *0-junction* on the bond graph. They may be represented as,

$$P_{sv2} = u(P_{sv}, P_{p1}, P_{p2}, x_v, Q_{rl}) \tag{12}$$

$$P_{rl} = v(P_{sv}, P_{p1}, P_{p2}, x_v, Q_{rl}) \tag{13}$$

It can be noted that some differences between this model and that of [11] is the leakage between the chambers of the rotary actuator, whereas the focus of the previous work is a linear actuator. A second difference is the resistance introduced between supply line and the valve tip. In the suspension type valve, the supply flow impinges the valve tip and diverts to the control ports (see Figure 1). This introduces two stages of leakage from P_{sv} to P_{rl} and from P_{sv2} to P_{rl}. Furthermore, orifice areas as a function of the valve tip position differ from the those studied in [11]. Essentially, the orifice geometry is different. This is due to a different servovalve design.

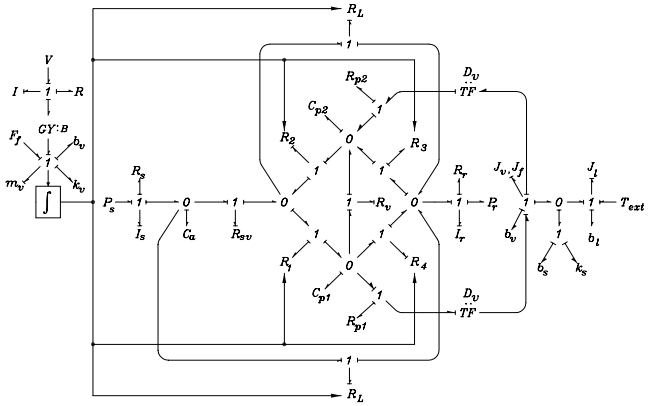

Fig. 2. System Bond Graph.

3 Parameter Identification

In order to obtain a reliable model of the servovalve and actuator, several parameters need to be identified. This information was obtained through experiments and consultation of handbooks and manufacturer's specifications. First, a description of the experimental setup is given.

3.1 Apparatus

The manipulator used is the slave of the SARCOS dexterous teleoperation system. The manipulator has ten degrees of freedom, seven in the arm and three in the hand. Joints are composed of single stage jet-pipe/suspension servovalves, and rotary or linear actuators. The elbow joint with its suspension type servovalve (model D3000H) and rotary actuator is used in order to identify and validate the model. Sensors onboard the robot, specifically, the elbow joint under study include an optical encoder angular position sensor, a rotary variable differential transformer (RVDT) for analog angular position measurement, and a strain-gage, full-bridge joint torque sensor.

Additional apparatus fabricated for identification of servovalve and actuator parameters include a steel brace to immobilize the elbow joint, three pressure transducers, a graduated cylinder, and a manifold equipped with pressure taps. The brace is designed and constructed for the study of the open-loop system in a static mode and can be used to validate static joint torque control, see Figure 3. The manifold is designed and built to allow access to the supply, return and the two control lines for pressure measurement, see Figure 4. For the manifold, the pressure transducers and the interface to the robot (middle right) are evident. By strategically blocking certain ports, a flow rate,

such as actuator leakage, may be measured by volume measurements over time. The usefulness of the equipment is three-fold: (1) identification, (2) validation of the model, and (3) possible use of pressure signals in a feedback loop. In addition, the manifold may be installed at other joints with similar servovalve/robot interface.

Fig. 3. Joint brace.

Fig. 4. Manifold.

3.2 Experiments

Several experiments were devised to identify as many individual parameters as possible. Some of these parameters include the shaft stiffness and the actuator volumetric displacement. The joint shaft stiffness was obtained by immobilizing the elbow joint with the joint brace and measuring torque and angular joint position. Plotting torque versus angular position an approximate straight line results whose slope is the angular joint stiffness, given in Figure 5. Here, the slope gives a joint stiffness of 8.9×10^4 lb·in/rad. Theoretically, assuming a solid shaft, the shaft stiffness is approximately given by,

$$k_s = \frac{GJ}{l_s} = 11.06\times10^4\, lb\cdot in/rad \qquad (14)$$

where, G is the shear modulus of the shaft material, J is the shaft moment of inertia and l_s is the shaft length.

Another key parameter is the actuator volumetric displacement since it relates the load flow to the angular velocity as well as the load pressure to the joint torque. These relations are given by,

$$Q_L = D_v\omega_{vn}, \text{ and } P_L = \frac{\tau}{D_v} \qquad (15)$$

With the manifold installed and the elbow free to rotate, a sinusoidal current was sent in open-loop resulting in an oscillation of the arm. With torque and pressure measurements, the torque vs. load pressure is plotted as shown in Figure 6. Here, the slope of the straight line segments is close to the ideal volumetric displacement of the rotary actuator, assuming external leakage of the actuator is small. The slope is found as $D_v = 0.288$ in^3/rad. The horizontal portions of the curve are due to the friction within the rotary actuator. The difference between the measured torque and the applied torque was used to identify the friction. Continuing, the actuator leakage between chambers can be found, with the elbow immobilized and measured pressures. This parameter is dependent on fluid viscosity and gap geometry, but here, for simplicity, it is assumed to be a constant denoted by R_v and it was estimated to be 8.24×10^{-5} in^5/lb-s.

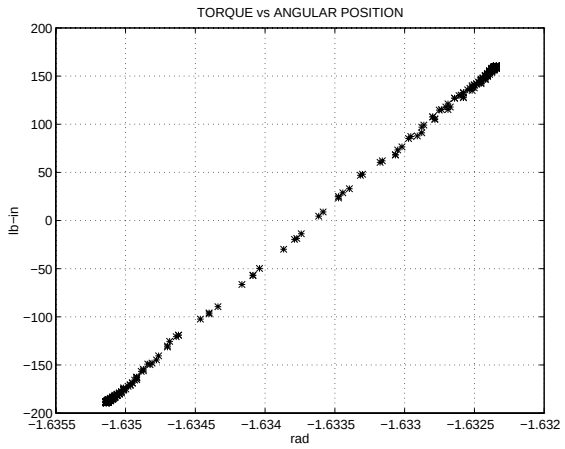

Fig. 5. Determination of shaft stiffness.

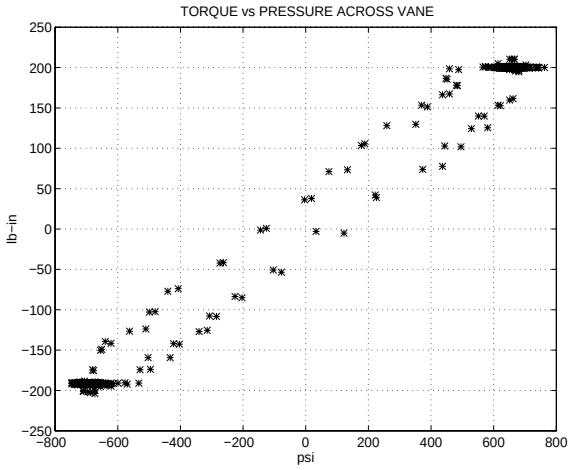

Fig. 6. Determination of actuator volumetric displacement.

Orifice geometry was obtained from photographs and orifice diameters were measured. As for the load parameters, they were obtained by a least squares estimation and static measurements. Those parameters that were not estimated with good certainty include the clearance between valve tip and receiver. In these cases, these parameters were tuned until satisfactory correlation between simulation and experiments was obtained.

4 Validation

To verify the model, both static and dynamics tests were performed in simulation and compared to experimental

results. The simulations were done using *s-function* approach in Matlab with the Gear integration method. Experiments were performed in open-loop mode at an operating supply pressure of 3000 psi. Results were sampled at 0.1 seconds.

4.1 Static Case

For different constant input currents of 0.05 A and 0.10 A, the chamber pressures and supply pressure before the servovalve are shown in Figures 7 and 8 respectively.

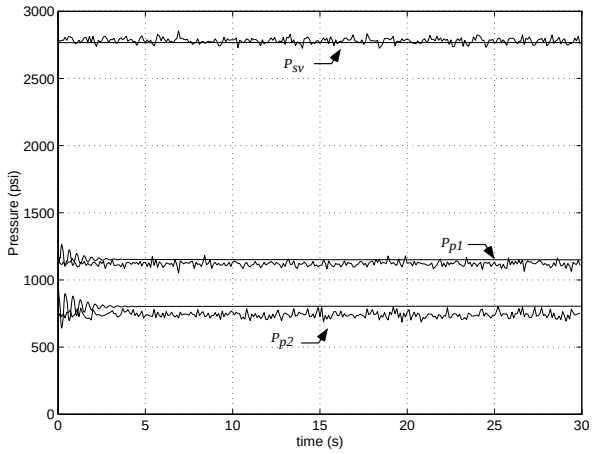

Fig. 7. Supply Pressure before Servovalve, and Chamber Pressures for i = 0.05 A.

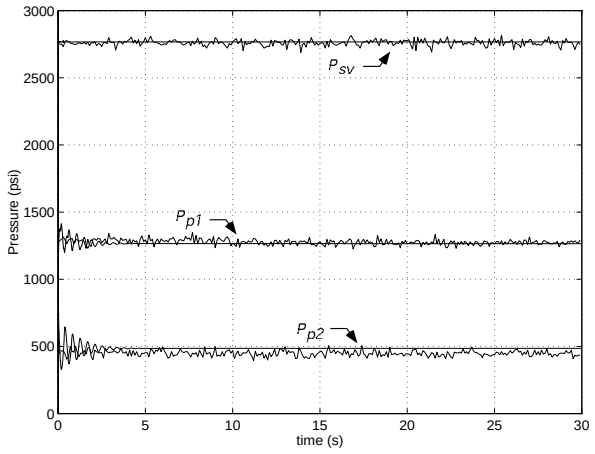

Fig. 8. Supply Pressure before Servovalve, and Chamber Pressures for i = 0.1 A.

Our interest is in the steady state which can be seen to be beyond 10 seconds. The model faithfully describes the system in static mode. The experimental steady state results are those after inputting a sinusoid current with an exponentially decreasing amplitude in order to avoid the hysteresis effect. Illustrated in Figure 9 is the load position in simulation and experiment. Initial conditions were set to those of the experiment after steady state was reached.

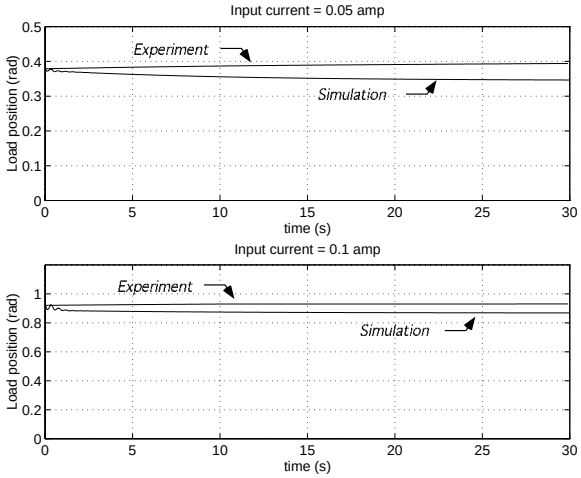

Fig. 9. Load angle for i = 0.1 A and for i = 0.05 A.

4.2 Dynamic Case

To verify the dynamic performance of the model, a sinusoidal current is used as the input to the open-loop system, so the arm rotates about the elbow in the vertical plane. The input current is given as,

$$i = 0.1\sin(0.25t) \qquad (16)$$

With the initial conditions for the simulation set to those of the actual system, supply pressure before the servovalve, and chamber pressures were measured. Figure 10 shows the plots with respect to time. As it can be seen, the model predicts well the pressure response.

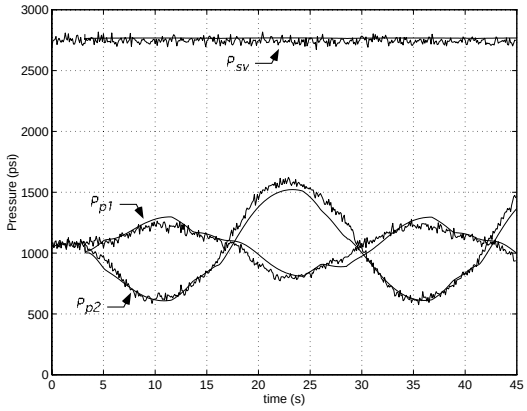

Fig. 10. Supply and Chamber Pressures: Simulation and Experiment.

Of importance in force control is the load pressure, the difference between the chamber pressures. It's time history is shown in Figure 11. Good agreement between simulation results and experimental results is evident. The response of the load position, illustrated in Figure 12, compares well to the experimental load position. Results indicate the stick-slip friction model is satisfactory as well as the dynamic parameters of the load. Overall, the model predicts well the angular position of the load.

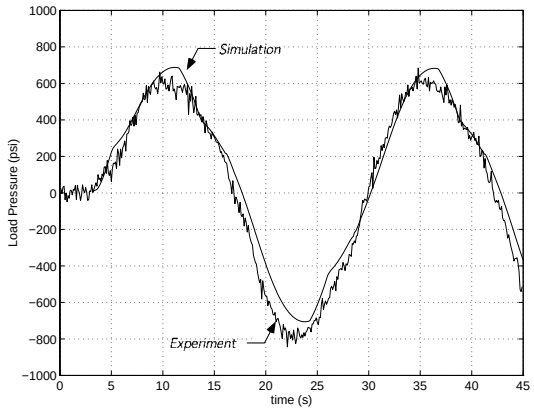

Fig. 11. Load pressure: simulation & experiment.

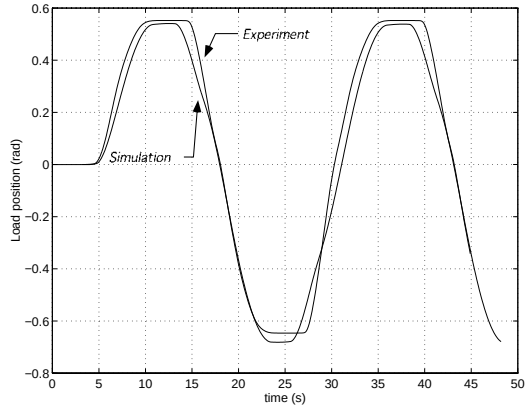

Fig. 12. Load angle: simulation & experiment.

Some differences between simulation and experiments do exist due to unmodelled effects and due to the lumped parameter approach in modelling. Some of these factors include the reduction of oil bulk modulus due to air entrainment, temperature variation of oil properties, and the losses in the numerous elbows and fittings in the oil passages (essentially they were assumed to be lumped together). From the results, they do not seem to be significant for the purpose of control, since the goal of the model is to reduce control effort.

5 Conclusions

An accurate model of a hydraulic joint of a manipulator has been presented. The model follows closely experimental results. The model accounts for the major effects of an electrohydraulic actuator such as hysteresis, flow through orifices, and line losses. This model can be extended to other joints of the SARCOS slave manipulator as well as the master in such a way as to obtain a complete model of the hydraulics of the SARCOS manipulator. Modifications need to be made for those joints having the smaller model of servovalve and linear actuators. In all, the model represents well the behaviour of the real system. It is expected that this model will be useful in control design by reducing control effort and will allow improvements to control performance.

6 Acknowledgments

The support of this work by the Fonds pour la Formation de Chercheurs et l'Aide a la Recherche (FCAR), and by the Natural Sciences and Engineering Council of Canada (NSERC) is gratefully acknowledged.

References

[1] Blackburn, J.F., Reethof, G., and Shearer, J.L., ed. *Fluid Power Control*, Cambridge: The M.I.T. Press, 1960.

[2] Bluethmann, B., et. al., "Experiments in Dexterous Hybrid Force and Position Control of a Master/Slave Electrohydraulic Manipulator," *IEEE/RSJ International Conference on Intelligent Robots and Systems*, Vol. 3, pp. 27-32, 1995.

[3] Boulet, B., et. al., "Characterization, Modeling and Identification of a High Performance Hydraulic Actuator for Robotics," *CIM report TR-CIM-93-9*, McGill University, March 1993.

[4] Carpenter, K.H., "A Differential Equation Approach to Minor Loops in the Jiles-Atherton Hysteresis Model," *IEEE Transactions on Magnetics*, Vol. 27, No. 6, pp. 4404-4406, 1991.

[5] Dunnigan, M.W., et. al., "Hybrid Position/Force Control of a Hydraulic Underwater Manipulator," *IEE Proceedings: Control Theory and Applications*, Vol. 143, No. 2, pp. 145-151, March 1996.

[6] Heinrichs, B., Sepehri, N., & Thornton-Trump, A.B., "Position-Based Impedance Control of an Industrial Hydraulic Manipulator," *Proc. IEEE Int. Conf. on Robotics & Autom.*, pp. 284-290, 1996.

[7] Heintze, J., et. al., "Modeling and control of an industrial hydraulic rotary vane actuator," *Proc. of the 32nd Conference on Decision and Control*, San Antonio, TX, pp. 1913-1918, December 1993.

[8] Karnopp, D.C., Margolis, D.L., and Rosenberg, R.C., *System Dynamics: A Unified Approach*, New York: John Wiley and Sons, 2nd ed., 1990.

[9] Kwon, D.S., et. al., "Tracking Control of the Hydraulically Actuated Flexible Manipulator," *Proc. IEEE International Conference on Robotics and Automation*, pp. 2200-2205, 1995.

[10] Laval, L., M'Sirdi, N.K., and Cadiou, J-C., "H∞-Force Control of a Hydraulic Servo-Actuator with Environmental Uncertainties," *Proc. IEEE Int. Conf. on Robotics & Autom.*, pp. 1566-1571, 1996.

[11] McLain, T.W., et. al., "Development, Simulation, and Validation of a Highly Nonlinear Hydraulic Servosystem Model," Proceedings of the American Control Conference, (Pittsburgh, Pennsylvania), pp. 385-391, June 1989.

[12] Merrit, H.E., Hydraulic Control Systems, New York: John Wiley and Sons Inc., 1967.

[13] Unruh, S., et. al., "A hybrid position/force and positional accuracy controller for a hydraulic manipulator," *SPIE Telemanipulator & Telepresence Technologies*, Vol. 2351, pp. 207-213, 1994.